AE4304P: Stochastic Aerospace System Practical

Analysis of simulated aircraft responses to atmospheric turbulence

José Cunha - 5216087

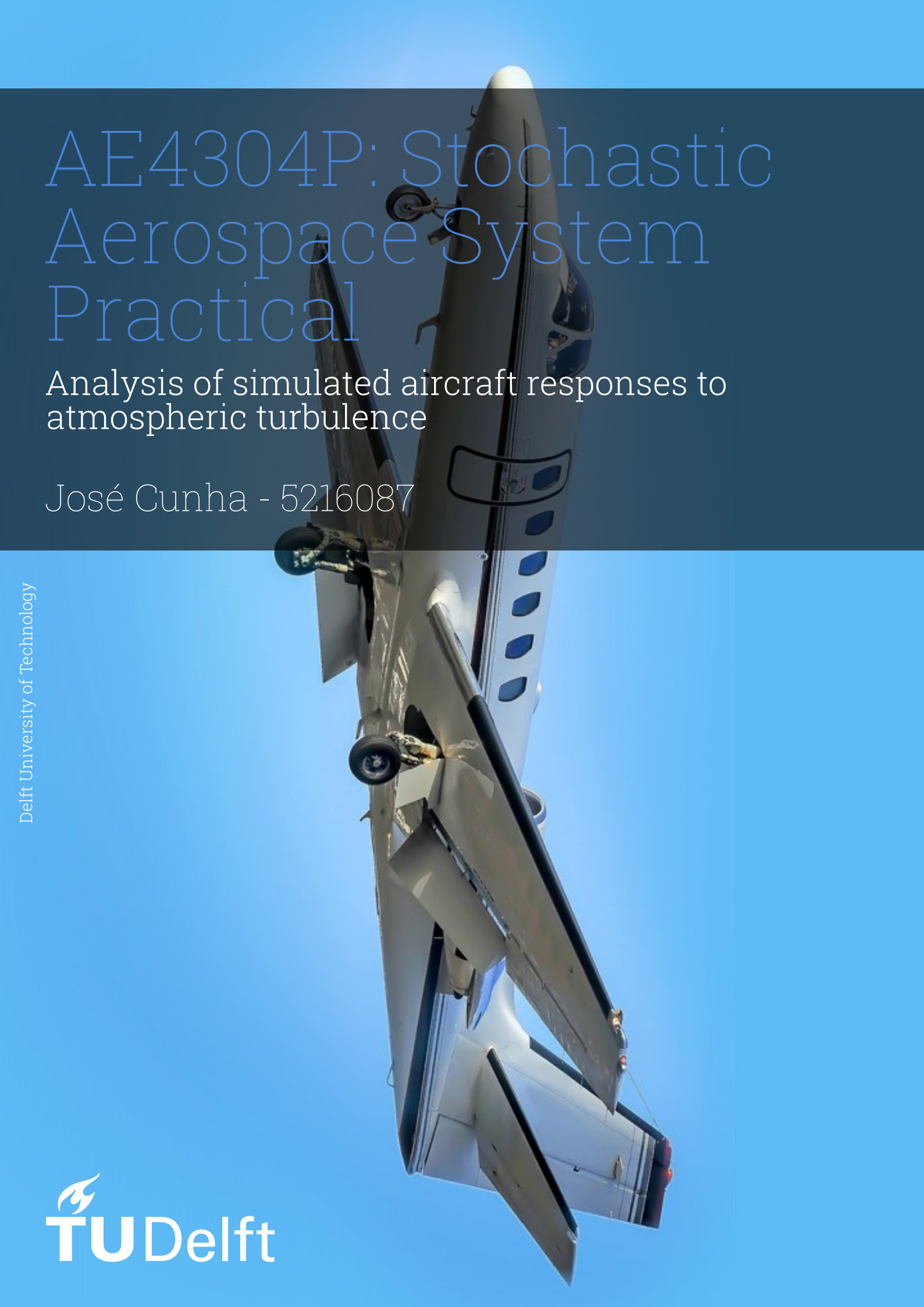

Delft University of Technology

TU Delft

Contents

1

Introduction

The aim of this report is to simulate the response of a Citation aircraft to atmospheric turbulence. The report focuses on the symmetric aircraft response to vertical turbulence, for the aircraft with and without the pitch damper activated. It is divided into three main sections: stability and time-domain analysis, spectral analysis and variance calculation. The stability and time-domain analysis section models the response of the Citation aircraft to atmospheric turbulence, using an LTI state-space system. The spectral analysis section focuses on the power spectral density (PSD) functions of the relevant aircraft states, calculated both analytically and experimentally. The variances section calculates the variances of the aircraft states using three different methods.

2

Stability and Time-Domain Anaysis

2.1. Aircraft response

To model the response of Citation, an LTI state-space system was constructed, namely for symmetric motion. The dynamics equation of this state-space can be seen in Equation 2.1. For the output equation, it is assumed that the system is fully observable (i.e. the output matrix C is the identity) and has no feedthrough (matrix D is the zero matrix).

$$\begin{bmatrix} \dot{\hat{u}} \\ \dot{\alpha} \\ \dot{\theta} \\ \frac{\dot{q}\bar{c}}{V} \\ \dot{\hat{u}}_g \\ \dot{\alpha}_g \\ \dot{\alpha}_g^* \end{bmatrix} = \begin{bmatrix} x_u & x_\alpha & x_\theta & 0 & x_{u_g} & x_{\alpha_g} & 0 \\ z_u & z_\alpha & z_\theta & z_q & z_{u_g} - z_{\dot{u}_g}\frac{V}{L_g}\frac{\bar{c}}{V} & z_{\alpha_g} & z_{\dot{\alpha}_g}\frac{\bar{c}}{V} \\ 0 & 0 & 0 & \frac{V}{\bar{c}} & 0 & 0 & 0 \\ m_u & m_\alpha & m_\theta & m_q & m_{u_g} - m_{\dot{u}_g}\frac{V}{L_g}\frac{\bar{c}}{V} & m_{\alpha_g} & m_{\dot{\alpha}_g}\frac{\bar{c}}{V} \\ 0 & 0 & 0 & 0 & -\frac{V}{L_g} & 0 & 0 \\ 0 & 0 & 0 & 0 & 0 & 0 & 1 \\ 0 & 0 & 0 & 0 & 0 & -\frac{V^2}{{L_g}^2} & -2\frac{V}{L_g} \end{bmatrix} \begin{bmatrix} \hat{u} \\ \alpha \\ \theta \\ \frac{q\bar{c}}{V} \\ \hat{u}_g \\ \alpha_g \\ \alpha_g^* \end{bmatrix} + \\ + \begin{bmatrix} x_{\delta_e} & 0 & 0 \\ z_{\delta_e} & z_{\dot{u}_g}\frac{\bar{c}}{V}\sigma_{\hat{u}_g}\sqrt{\frac{2V}{L_g}} & z_{\dot{\alpha}_g}\frac{\bar{c}}{V}\sigma_{\alpha_g}\sqrt{\frac{3V}{L_g}} \\ 0 & 0 & 0 \\ m_{\delta_e} & m_{\dot{u}_g}\frac{\bar{c}}{V}\sigma_{\hat{u}_g}\sqrt{\frac{2V}{L_g}} & m_{\dot{\alpha}_g}\frac{\bar{c}}{V}\sigma_{\alpha_g}\sqrt{\frac{3V}{L_g}} \\ 0 & \sigma_{\hat{u}_g}\sqrt{\frac{2V}{L_g}} & 0 \\ 0 & 0 & \sigma_{\alpha_g}\sqrt{\frac{3V}{L_g}} \\ 0 & 0 & (1-2\sqrt{3})\sigma_{\alpha_g}\sqrt{\left(\frac{V}{L_g}\right)^3} \end{bmatrix} \begin{bmatrix} \delta_e \\ w_1 \\ w_3 \end{bmatrix} \tag{2.1}$$

All the control derivatives were calculated from the aircraft data given in the assignment (seen in Table A.1). The A and B can then be found from them resulting in Equation 2.2 below.

$$A = \begin{bmatrix} -0.0363 & 0.0785 & -0.1900 & 0 & -0.0363 & 0.0785 & 0 \\ -0.3765 & -0.8501 & 0 & 24.5512 & -0.3765 & -0.8501 & 0.0159 \\ 0 & 0 & 0 & 25.4204 & 0 & 0 & 0 \\ 0.0091 & -0.0476 & -0.0046 & -1.8501 & 0.0091 & -0.0476 & 0.0247 \\ 0 & 0 & 0 & 0 & -0.0343 & 0 & 0 \\ 0 & 0 & 0 & 0 & 0 & 0 & 1.0000 \\ 0 & 0 & 0 & 0 & 0 & -0.0012 & -0.0685 \end{bmatrix}$$

$$B = \begin{bmatrix} 0 & 0 & 0 \\ -0.1034 & 0 & 0.0002 \\ 0 & 0 & 0 \\ -0.2625 & 0 & 0.0003 \\ 0 & 0.0102 & 0 \\ 0 & 0 & 0.0125 \\ 0 & 0 & -0.0006 \end{bmatrix} \tag{2.2}$$

To analyse the stability of the aircraft, the eigenvalues of A can be calculated, where the system is said to be stable if $\mathcal{R}(\lambda_i) < 0 \quad \forall i$, where λ_i is an eigenvalue of A. These can be seen in Figure 2.1 and Table 2.1

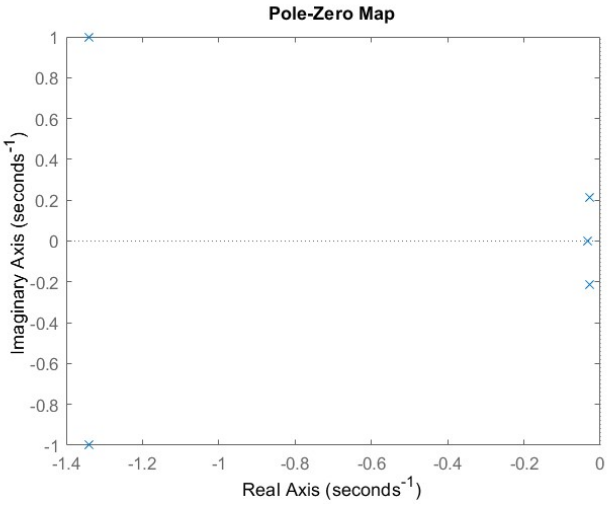

Figure 2.1: *Pole zero map of system.*

Table 2.1: *Eigenvalues of* A

Eigenvalues
$-1.34 + 0.9959i$
$-1.34 - 0.9959i$
$-0.0283 + 0.2151i$
$-0.0283 - 0.2151i$
-0.0343

Looking at Table 2.1, one can determine that the system will be stable as all the eigenvalues have a negative real part (for both the phugoid and short-period eigenmodes). This can also be observed from the response of the states, especially in the pitch rate (seen in Figure 2.2), where for both eigenmotions it is damped down.

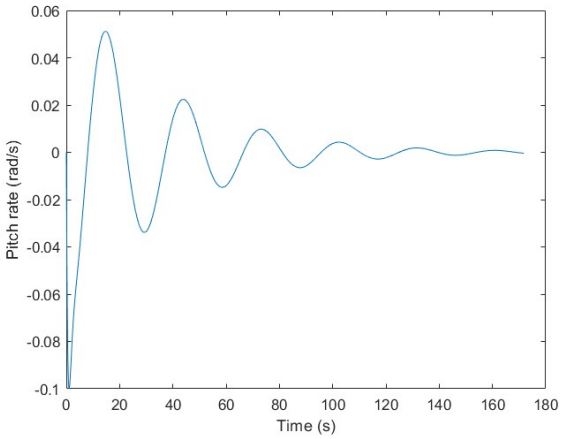

(a) *Pitch rate response after a step elevator input, causing the phugoid eigenmotion.*

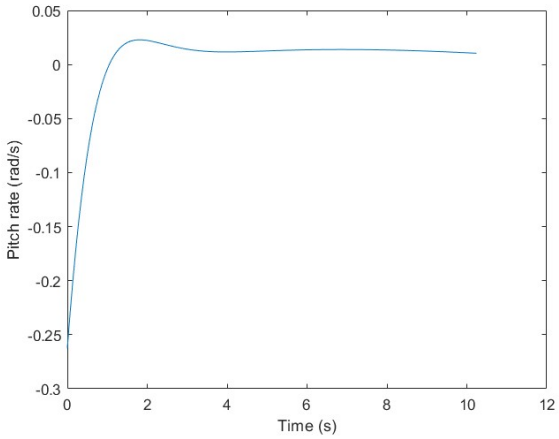

(b) *Pitch rate response after an impulse elevator input, causing the short-period eigenmotion.*

Figure 2.2

Now, a pitch damper can be included, which uses the control law $\delta_e = K_\theta \theta$ when the autopilot is

activated. The pitch gain has to be chosen such that the phugoid damping factor is $\zeta_{phugoid} \approx 0.5$. Through trial and error, the gain could be tuned until desired damping factor was achieved, which can be calculated from the eigenvalue according to Equation 2.3.

$$\zeta_{phugoid} = \frac{-\mathcal{R}(\lambda_{phugoid})}{|\lambda_{phugoid}|} \tag{2.3}$$

With this, the gain was found to be $K_\theta = -0.099$. This gain can be substituted into a gain matrix, which can be used to recalculate the state matrix A to include the pitch damper, seen in Equation 2.5.

$$K = \begin{bmatrix} 0 & 0 & -0.099 & 0 & 0 & 0 & 0 \\ 0 & 0 & 0 & 0 & 0 & 0 & 0 \\ 0 & 0 & 0 & 0 & 0 & 0 & 0 \end{bmatrix} \tag{2.4}$$

$$A_{damped} = A - BK \tag{2.5}$$

With this new state matrix, the stability of this pitch-damped state space system can be analysed, by again looking the the eigenvalues of the state matrix, which can be seen in the pole-zero map of Figure 2.3 and Table 2.2. It can be observed that again, the real part of all eigenvalues is negative - demonstrating that the system is stable - and now the eigenvalue corresponding to the phugoid eigenmotion has moved to the left on the complex plane, showing a more pronounced damping.

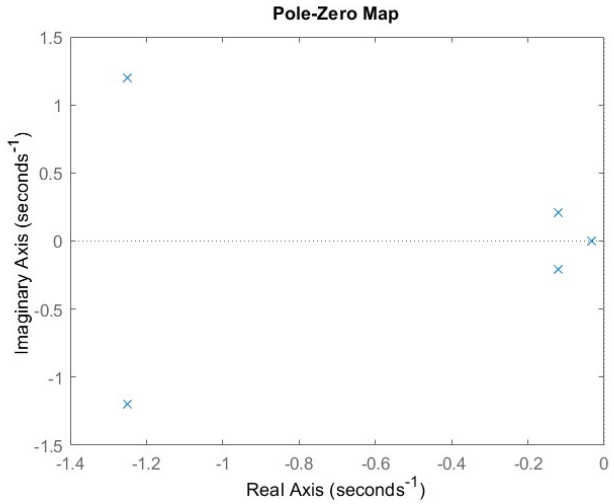

Figure 2.3: *Pole-zero map of the system with a pitch damper.*

Table 2.2: *Eigenvalues of* A_{damped}.

Eigenvalues
$-1.249 + 1.197i$
$-1.249 - 1.197i$
$-0.1193 + 0.2069i$
$-0.1193 - 0.2069i$
-0.0343

The damped pitch rate response can also be plotted for both eigenmotions, where it can be seen that the phugoid pitch rate has much greater damping ($\zeta_{phugoid} = 0.5$ as opposed to $\zeta_{phugoid} = 0.13$ in the system without pitch damper), while the phugoid is relatively unchanged. Both also show a convergence to a constant value demonstrating the stability of the system (seen in Figure 2.4).

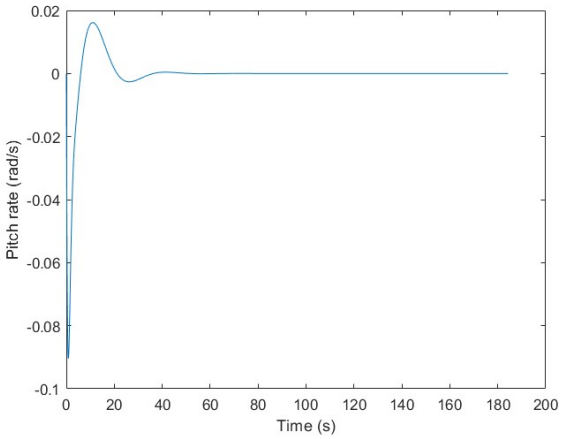

(a) *Pitch rate response after a step elevator input, causing the phugoid eigenmotion.*

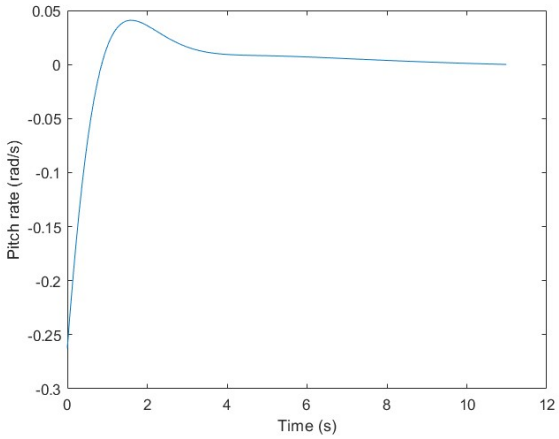

(b) *Pitch rate response after an impulse elevator input, causing the short-period eigenmotion.*

Figure 2.4: *State response to elevator input, with an activated pitch damper.*

2.2. Time-domain analysis

The aircraft response to vertical turbulence can be simulated by generating stochastic measurement data for the vertical gust velocities. The gust velocity is generated as white noise with intensity of one, and standard distribution $\sigma_{w_g} = 2\,\mathrm{m/s}$.

Moreover, an additional state was simulated, namely the vertical load factor n_z. This was calculated from the other aircraft states using Equation 2.6, and added to the state-space representation.

$$n_z = -\frac{a_z}{g} \approx \frac{V}{g}\dot{\gamma} \approx \frac{V}{g}(\dot{\theta} - \dot{\alpha}) \approx \frac{V}{g}(q - \dot{\alpha}) \tag{2.6}$$

With this, the time traces of the relevant aircraft states ($\hat{u}, \theta, \alpha, \frac{q\bar{c}}{V}$ and n_z) were simulated for both the uncontrolled and controlled (with pitch damper) aircraft. The results of these simulations can be found in Figure 2.5 and Figure 2.6.

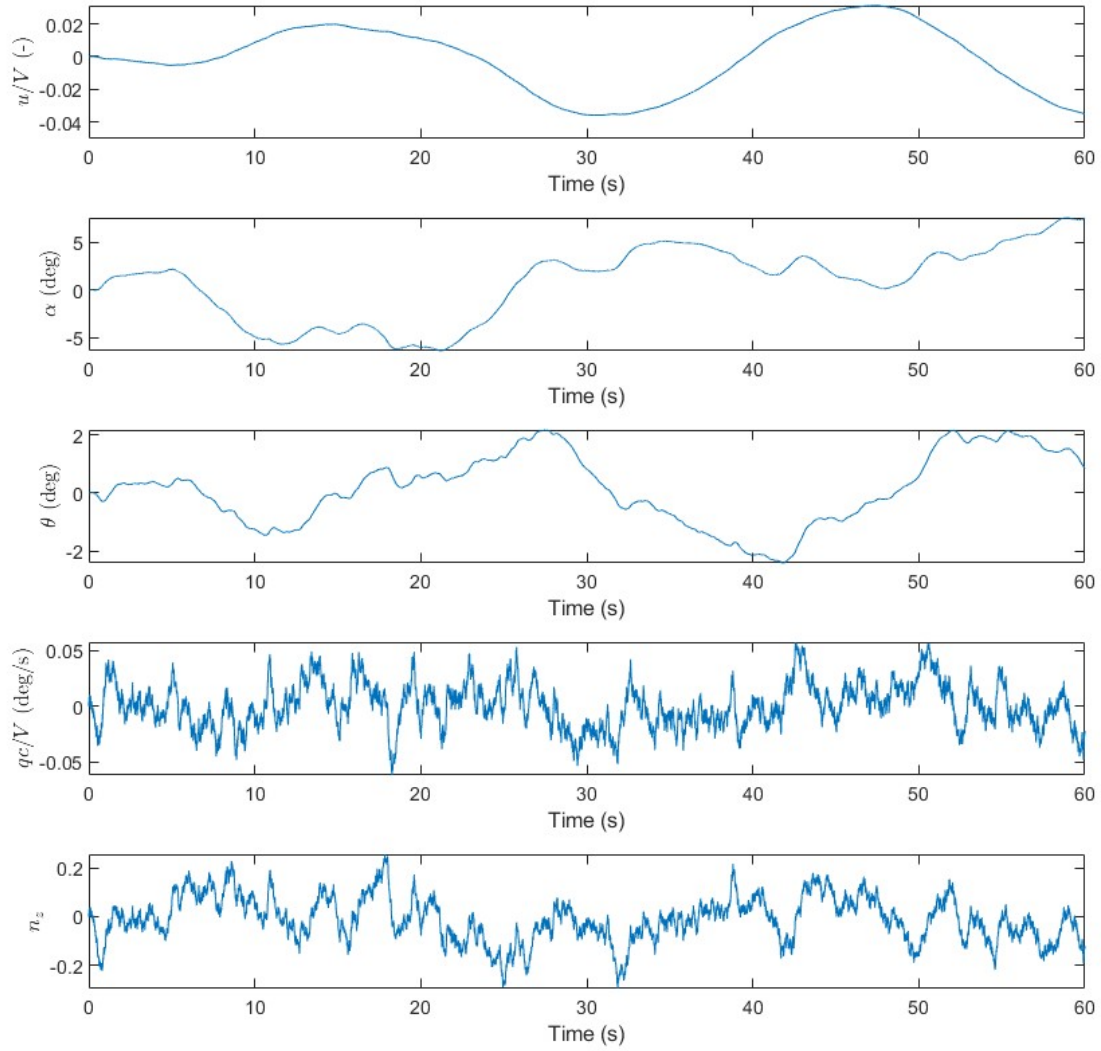

Figure 2.5: *Time traces of response of uncontrolled aircraft states to vertical turbulence.*

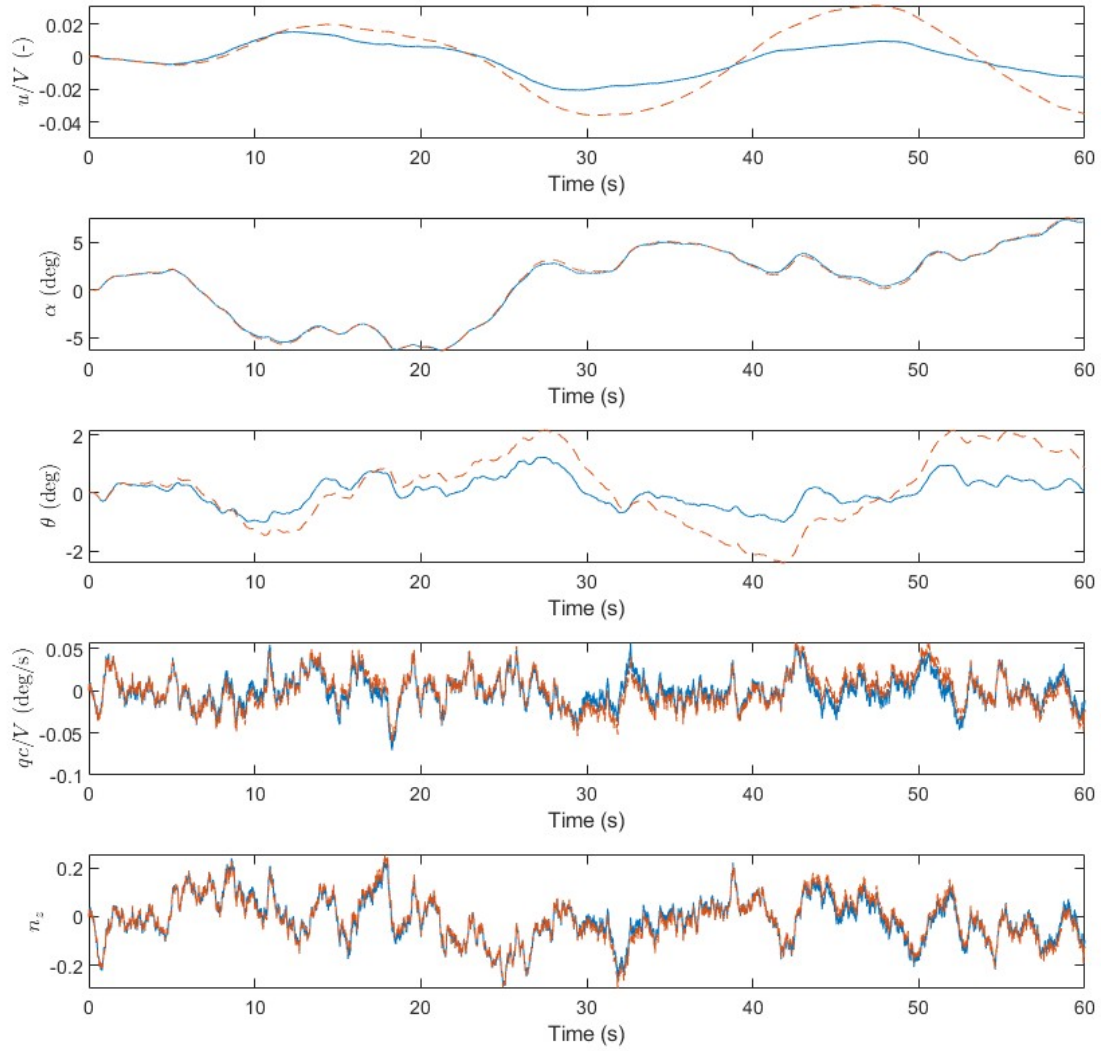

Figure 2.6: *Time traces of response of controlled aircraft states to vertical turbulence. Overlaid in red is are the time traces of the uncontrolled aircraft.*

3
Spectral Analysis

3.1. Analytic power spectral densities

The power spectral density (PSD) functions of each of the aircraft states can be calculated analytically, by considering the magnitude of the frequency response function to a white noise input (assumed to have unity intensity over the frequency range). This relationship can be seen Equation 3.1. The PSDs of the relevant states were calculated with and without the autopilot activated, seen in Figure 3.1 and Figure 3.2 respectively.

$$S_{x_i x_i}(w) = |H_{x_i w_3}(\omega)|^2 \cdot S_{w_3 w_3}(w) = |H_{x_i w_3}(\omega)|^2 \tag{3.1}$$

To calculate the power spectral density of the load factor state, its frequency response function could be calculated, referencing Equation 2.6, from the frequency response functions of the pitch rate and angle of attack rate, as seen in Equation 3.2.

$$S_{n_z n_z}(\omega) = |H_{n_z w_3}(\omega)|^2 = \left| \frac{V}{g} \left(\frac{V}{\bar{c}} H_{q w_3}(\omega) - H_{\dot{\alpha} w_3}(\omega) \right) \right|^2 \tag{3.2}$$

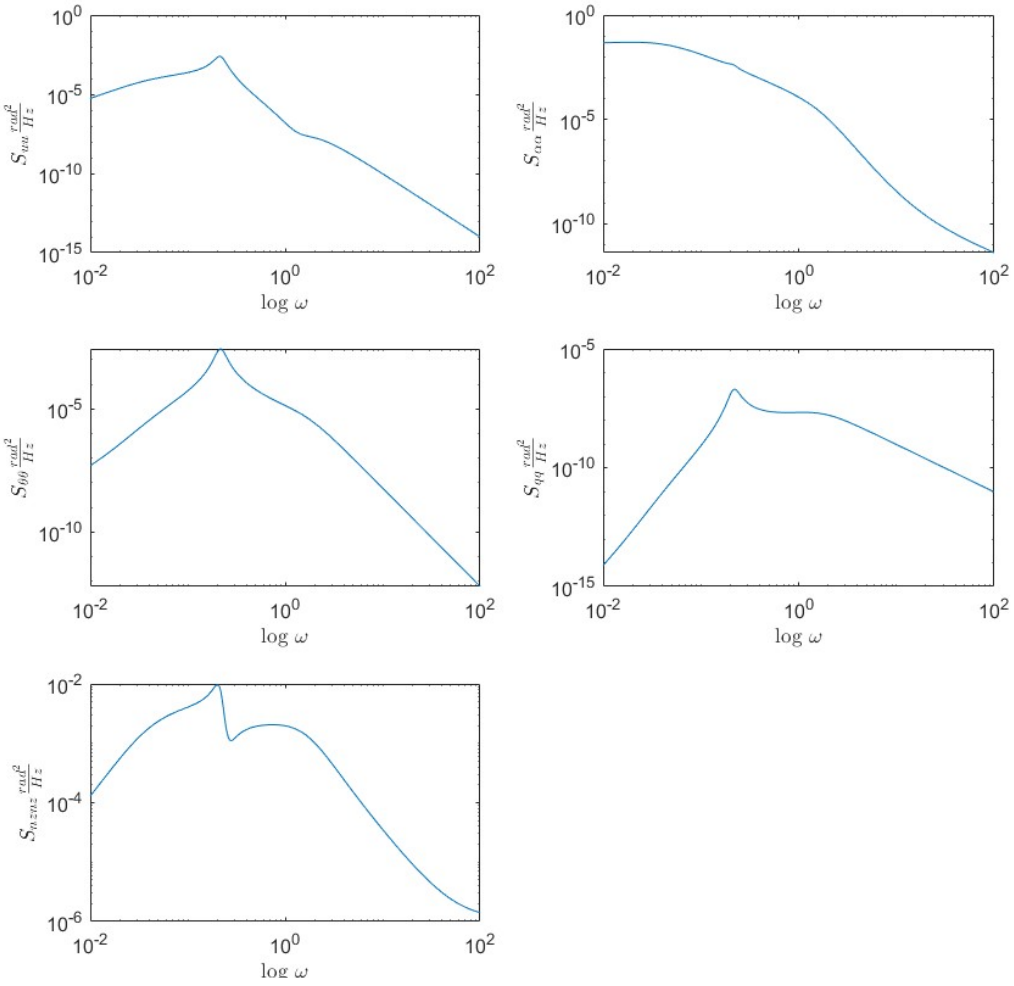

Figure 3.1: *Analytic PSDs for the five relevant aircraft states, without pitch damper.*

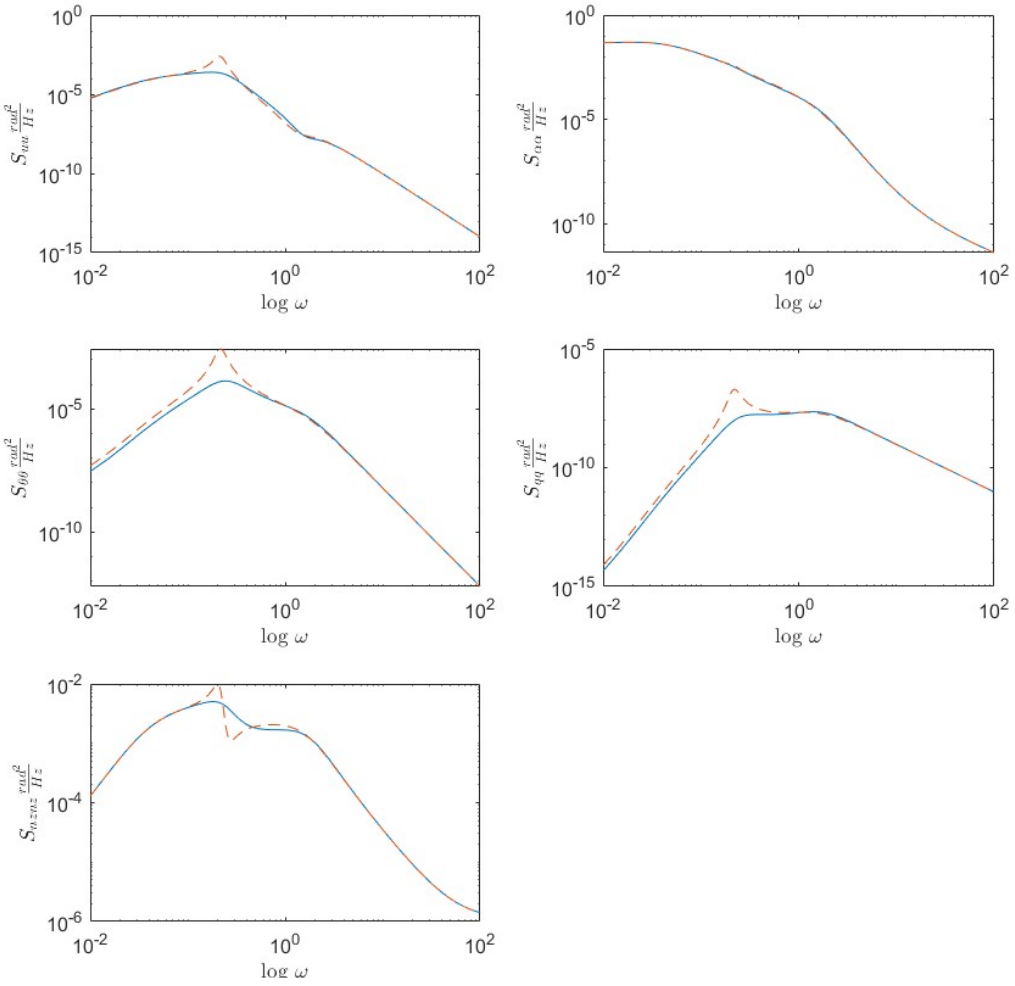

Figure 3.2: *Analytic PSDs for the five relevant aircraft states with the pitch damper activated. Overlaid in red are the PSDs without pitch damper.*

Comparing Figure 3.1 and Figure 3.2, the differences between the controlled and uncontrolled aircraft can be seen, notably in the $\hat{u}$, θ, $\frac{q\bar{c}}{V}$ and n_z states. In these states, the transient spike of the magnitude plots is reduced by the pitch-damper, which is precisely the use of the pitch-damper. It should be expected that the angle of attack is unaffected by the pitch-damper, as from the state matrix (Equation 2.2), the α state has no dependence on θ.

3.2. Experimental power spectral densities

In the previous section, the PSD functions were calculated analytically from the frequency response. However, these functions can also be calculated from the time-domain results directly. This comes from the fact that the PSD function can be estimated from discrete data in the form of a periodogram, which can be calculated using Equation 3.3.

$$I_{N_{xx}}[k] = \frac{1}{N} X^*[k] X[k], \tag{3.3}$$

where $X[k]$ is the Discrete Fourier Transform (DFT) of the time traces data. In this case, the DFT was calculated using MATLAB's `fft.m` function. The experimental periodograms for the relevant aircraft states, with both pitch damper off and on, can be seen in Figure 3.3 and Figure 3.4 respectively.

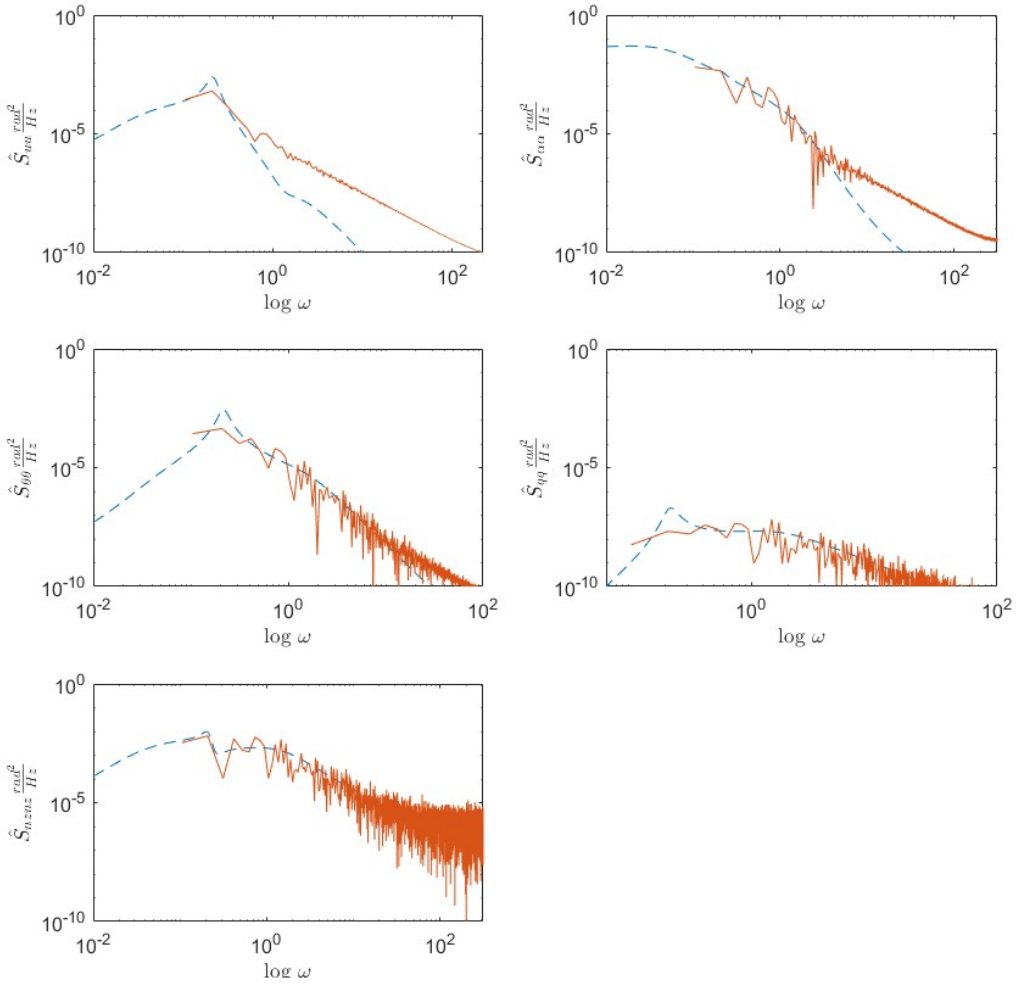

Figure 3.3: *Experimental PSDs (periodograms) for the five relevant aircraft, without pitch damper. Overlaid in blue are the analytic PSDs.*

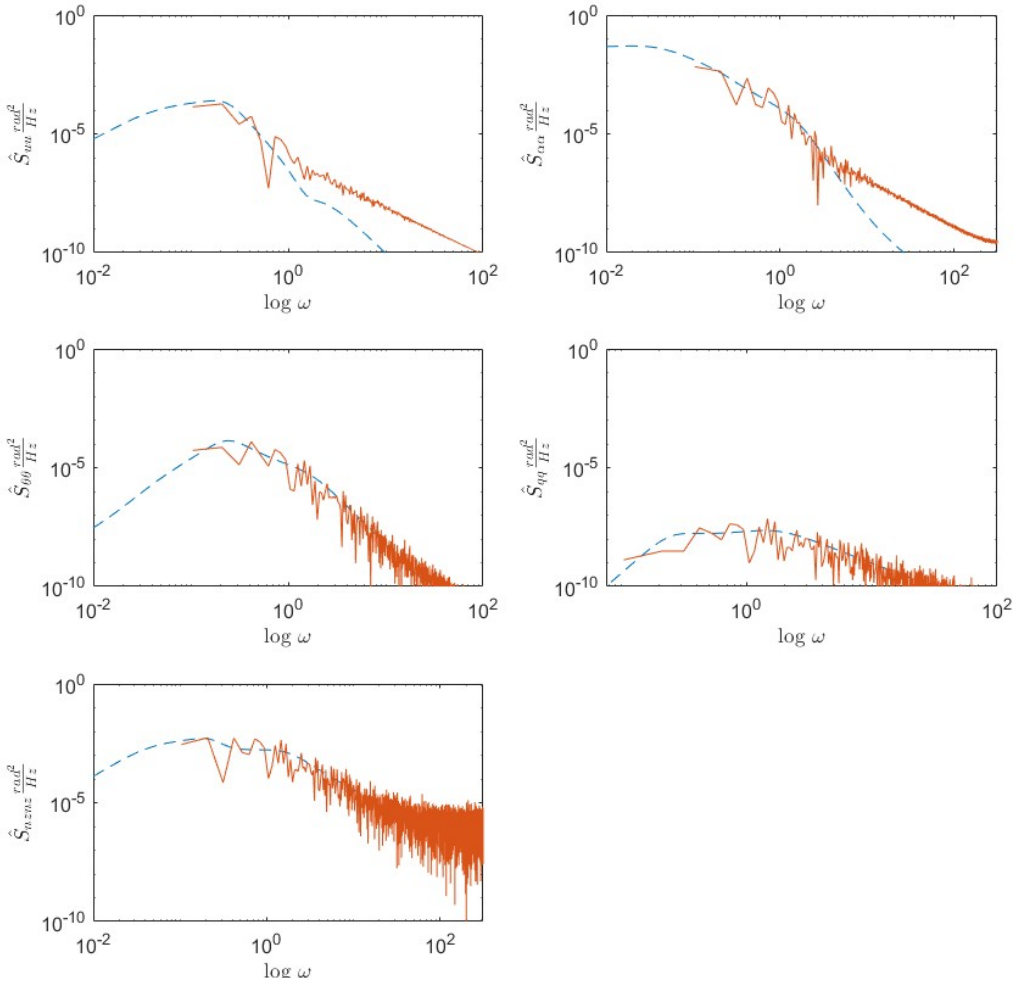

Figure 3.4: *Experimental PSDs (periodograms) for the five relevant aircraft, with pitch damper. Overlaid in blue are the analytic PSDs.*

Comparing the controlled from the uncontrolled aircraft (Figure 3.3 and Figure 3.4 respectively), the effect of the pitch damper on the periodograms cannot be clearly seen. This comes from the noise of the periodograms, making it hard to discern the small differences between the two aircraft.

To reduce the variance of the PSD estimate (periodogram), a smoothed estimator of the PSD can be calculated, in this case using MATLAB's `pwelch.m` function.

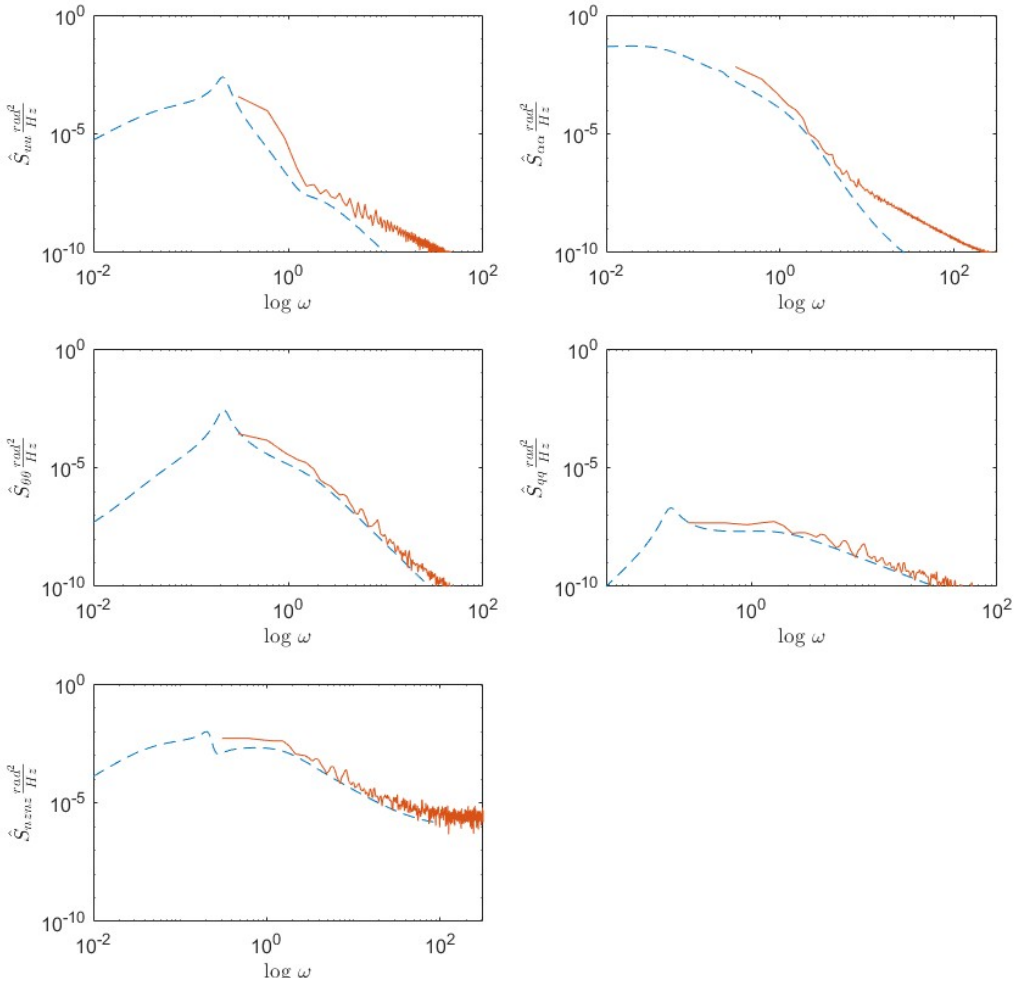

Figure 3.5: *Smoothed periodograms for the five relevant aircraft, without pitch damper. Overlaid in blue are the analytic PSDs.*

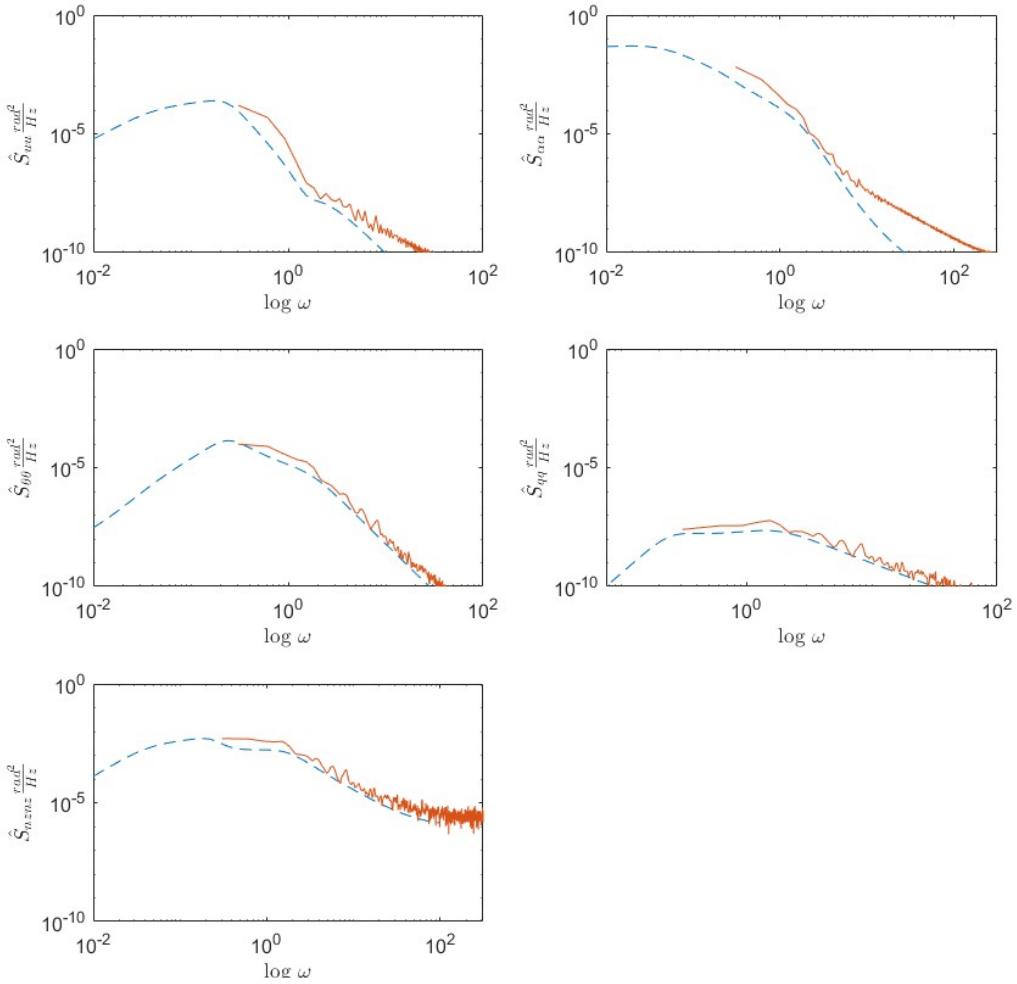

Figure 3.6: *Smoothed periodograms for the five relevant aircraft, with pitch damper. Overlaid in blue are the analytic PSDs.*

Similarly to the unsmoothed experimental PSDs, the differences between the controlled and uncontrolled aircraft are not readily apparent in the two smoothed periodograms of Figure 3.5 and Figure 3.6. Even though the Welch PSD estimate is less noisy than the previous method, the differences are not as apparent as with the analytic PSD.

Moreover, the differences between the two PSD estimation methods can be compared. Estimating the PSD from the discrete Fourier transform (DFT) yields not only noisier but less accurate results, while the second method using `pwelch.m` yields results that better follow the analytic results. This comes from the use of Welch's method to smooth the PSD estimate. This method is similar to the Bartlett method, wherein all samples are divided into K segments of M samples each, and the PSD estimate is calculated from the average of the K different periodograms. Welch's method differs from the Bartlett approach as it divides the samples into K overlapping segments, and then each segment is windowed in the time-domain[1]. This reduces the variance (and hence noise) of the estimate, at the cost of some frequency resolution.

[1]Otis M Solomon Jr. "PSD computations using Welch's method". In: *NASA STI/Recon Technical Report N* 92 (1991), p. 23584.

4 Variances

To calculate the variances of all the aircraft states, three different methods were used: MATLAB's internal `var.m` method, integration of the analytic power spectral densities (using Equation 4.1) and a crude integration of both the on-smoothed and smoothed periodograms (using Equation 4.2). These methods were used to calculate the variances for the two aircraft variants (no autopilot and pitch damped). The values for the variances are summarised in Table 4.1.

$$\sigma^2 = \frac{W}{\pi}\int_0^\infty |H(\omega)|^2 d\omega = \frac{W}{\pi}\int_0^\infty S_{xx}(\omega)d\omega \tag{4.1}$$

$$\hat{\sigma}^2 = \frac{W}{\pi}\sum_{k=0}^{N} I_{N_{xx}}[k]\Delta k \tag{4.2}$$

Table 4.1: *Estimate of the variances of aircraft states using different methods.*

Method	**Variance of State**				
	$\hat{u}$	α	θ	$\frac{q\bar{c}}{V}$	n_z
Analytical PSD	6.64×10^{-5}	1.37×10^{-3}	8.0×10^{-5}	3.03×10^{-8}	1.95×10^{-3}
Analytical PSD (damped)	1.90×10^{-5}	1.37×10^{-3}	1.82×10^{-5}	2.62×10^{-8}	1.88×10^{-3}
Experimental PSD	1.08×10^{-5}	5.98×10^{-4}	2.57×10^{-5}	2.88×10^{-8}	2.01×10^{-3}
Experimental PSD (damped)	6.29×10^{-6}	5.92×10^{-4}	1.42×10^{-5}	2.86×10^{-8}	1.96×10^{-3}
Smoothed periodogram	9.44×10^{-6}	1.02×10^{-3}	4.05×10^{-5}	5.97×10^{-8}	4.48×10^{-3}
Smoothed periodogram (damped)	7.44×10^{-6}	1.01×10^{-3}	2.72×10^{-5}	6.01×10^{-8}	4.35×10^{-3}
MATLAB `var.m`	1.0×10^{-5}	3.04×10^{-4}	2.57×10^{-5}	2.87×10^{-8}	2.01×10^{-3}
MATLAB `var.m` (damped)	6.15×10^{-6}	2.97×10^{-4}	1.42×10^{-5}	2.86×10^{-8}	1.98×10^{-3}

From Table 4.1, one can observe that for all aircraft states, irrespective of the method chosen to calculate the variance of the signals, the values of the variance are quite similar. For all methods and states, the variance of the undamped aircraft is equal to or lower than that of the damped configuration. This occurs because for the states greatly affected by the damper (namely $\hat{u}, \theta$ and $\frac{q\bar{c}}{V}$) the transients of the signals are reduced, directly leading to a lower variance in the signal. For the other sates, where the damping does not affect the PSD, the variance did not (or barely) changed.

Considering the difference between the variance calculation methods, it is interesting to note that calculating the variance from the PSD estimate (periodogram) yielded lower variances than calculating using the analytical PSD. This is unexpected, since the periodograms are noisy estimates of the analytic spectra. However, since the periodograms are not calculated for the same full range as the analytic PSDs, this may account for the difference. Furthermore, regarding the differences between the periodograms and the smoothed PSD estimator methods, it is strange to see that the smoothed

periodograms yield a higher variance than their unsmoothed counterparts. This may be caused by the stochastic nature of the model, where a Monte Carlo-style averaging could have removed some of the outlier values of the variance.

5
Conclusion

In sum, the aim of this report, which was to simulate the response to an aircraft to atmospheric turbulence, was met. A model of the aircraft, made using the configuration and stability/control derivatives given in Appendix A was used to simulate the responses of the symmetric aircraft states to vertical turbulence. The responses were analyzed in both the time and frequency domains, for two different autopilot configurations: with and without a pitch-damper. Several components of the AE4304 course can be seen applied in this report, namely the calculation of the power spectral densities analytically, and the estimation of the same spectra (using the discrete Fourier transform to calculate the periodograms and Welch's method to smooth the periodograms). Finally, the variances of the aircraft states were calculated for these various analyses and compared.

Bibliography

[1] Otis M Solomon Jr. “PSD computations using Welch’s method”. In: *NASA STI/Recon Technical Report N* 92 (1991), p. 23584.

A
Appendix

Table A.1: *Stability and control derivatives of aircraft.*

Aircraft : Cessna Ce500 Citation I									
Configuration : landing									
$x_{c.g.}$	=	0.30	$\bar{c}$						
W	=	44675	N	V	=	51.4	m/sec	μ_b	= 11
m	=	4556	kg	h	=	0	m	K_X^2	= 0.012
S	=	24.2	m^2	ρ	=	1.225	kg/m^3	K_Z^2	= 0.037
$\bar{c}$	=	2.022	m	μ_c	=	76		K_{XZ}	= 0.002
b	=	13.36	m	l_h	=	5.5	m	K_Y^2	= 0.980
C_{X_0}	=	0		C_{Z_0}	=	-1.1360			
C_{X_u}	=	-0.2173		C_{Z_u}	=	-2.2720		C_{m_u}	= 0
C_{X_α}	=	0.4692		C_{Z_α}	=	-5.1300		C_{m_α}	= -0.4000
				$C_{Z_{\dot{\alpha}}}$	=	-1.4050		$C_{m_{\dot{\alpha}}}$	= -3.6150
C_{X_q}	=	0		C_{Z_q}	=	-3.8400		C_{m_q}	= -7.3500
C_{X_δ}	=	0		C_{Z_δ}	=	-0.6238		C_{m_δ}	= -1.5530
C_{Y_β}	=	-0.9896		C_{ℓ_β}	=	-0.0772		C_{n_β}	= 0.1628
C_{Y_p}	=	-0.0870		C_{ℓ_p}	=	-0.3415		C_{n_p}	= -0.0108
C_{Y_r}	=	0.4300		C_{ℓ_r}	=	0.2830		C_{n_r}	= -0.1930
$C_{Y_{\delta_a}}$	=	0		$C_{\ell_{\delta_a}}$	=	-0.2349		$C_{n_{\delta_a}}$	= 0.0286
$C_{Y_{\delta_r}}$	=	0.3037		$C_{\ell_{\delta_r}}$	=	0.0286		$C_{n_{\delta_r}}$	= -0.1261